Characteristics of Tropical Cyclone Rapid Intensification over the Western North Pacific

HIRONORI FUDEYASU

Yokohama National University, Yokohama, Japan

KOSUKE ITO

University of the Ryukyus, Nishihara, Japan

YOSHIAKI MIYAMOTO

Keio University, Fujisawa, and RIKEN, Kobe, Japan

(Manuscript received 29 September 2017, in final form 8 August 2018)

ABSTRACT

This study statistically investigates the characteristics of tropical cyclones (TCs) undergoing rapid intensification (RI) in the western North Pacific in the 37 years from 1979 to 2015 and the relevant atmospheric and oceanic environments. Among 900 TCs, 201 TCs undergoing RI (RI-TCs) are detected by our definition as a wind speed increase of 30 kt (15.4 m s^{-1}) or more in a 24-h period. RI-TCs potentially occur throughout the year, with low variation in RI-TC occurrence rate among the seasons. Conversely, the annual occurrence of RI-TC varies widely. In El Niño years, TCs tend to undergo RI mainly as a result of average locations at the time of tropical storm formation (TSF) being farther east and south, whereas TCs experience RI less frequently in La Niña years. The occurrence rates of RI-TC increased from the 1990s to the late 2000s. The RI onset time is typically 0–66 h after the TSF and the duration that satisfies the criteria of RI is 1–2 days. RI frequently occurs over the zonally elongated area around the eastern Philippine Sea. The development stage and life-span are longer in RI-TCs than in TCs that do not undergo RI. RI-TCs are small at the time of TSF and tend to develop as intense TCs as a result of environmental conditions favorable for TC development, weak vertical wind shear, high convective available potential energy, and tropical cyclone heat potential. The occurrence rates of RI-TCs that make landfall in Japan and the Philippines are higher than in China and Vietnam.

1. Introduction

Statistical analyses have shown that most category 4 and 5 Atlantic hurricanes undergo rapid intensification (RI) during their lifetimes (Kaplan and DeMaria 2003). Once a tropical cyclone (TC) begins RI, the TC attains a strong intensity (Lee et al. 2016). Hence, predicting RI is critically important for disaster prevention. However, RI prediction remains a significant challenge (Rappaport et al. 2012; Ito 2016).

Strong TCs typically experience two intensifying periods: an initial slow intensification and subsequent RI (e.g., Sitkowski and Barnes 2009). The intensification rate of the TC strongly depends on diabatic heating in the core region (e.g., Schubert and Hack 1982), and heating within the radius of maximum wind (RMW) intensifies the TC more efficiently (e.g., Shapiro and Willoughby 1982; Pendergrass and Willoughby 2009; Vigh and Schubert 2009; Ito et al. 2011; Fudeyasu and Wang 2011; Rogers et al. 2013). Furthermore, a larger symmetric heating component favors TC intensification (Nolan and Grasso 2003; Nolan et al. 2007). Many observational and modeling studies have shown that symmetric cloud structure is dominant inside the RMW during RI (Guimond et al. 2010; Harnos and Nesbitt 2011; Kieper and Jiang 2012; Jiang 2012; Miyamoto and Takemi 2013, 2015; Wang and Wang 2014; Zawislak et al. 2016; Rogers et al. 2013, 2016; Chang and Wu 2017; Shimada et al. 2017; Miyamoto and Nolan 2018). Modeling studies have indicated that TCs intensify through feedback between symmetric convection in the core and low-level mass convergence during RI, as described in

Corresponding author: H. Fudeyasu, fude@ynu.ac.jp

DOI: 10.1175/JCLI-D-17-0653.1

classical theories (Miyamoto and Takemi 2013, 2015; Chang and Wu 2017). Conversely, other studies show asymmetric convection is more distinct in the downshear side than symmetric convection (e.g., Molinari and Vollaro 2010; Chen et al. 2011; Nguyen and Molinari 2012; Zhang and Chen 2012; Chen and Zhang 2013; Chen and Gopalakrishnan 2015; Miller et al. 2015).

A pioneering study of RI by Kaplan and DeMaria (2003) identified large-scale characteristics of TCs undergoing RI (RI-TCs) in the North Atlantic, using the Statistical Hurricane Intensity Prediction Scheme (SHIPS) database. This statistical study was followed by those, including Kaplan et al. (2010, 2015) and Rozoff and Kossin (2011), who examined these large-scale characteristics for the Atlantic and eastern North Pacific basins. In particular, these studies showed that the occurrence of RI-TCs depends on environmental parameters such as a large intensity change during the previous 12 h, weak vertical wind shear, high relative humidity, large ocean heat content, large upper-level divergence, high symmetric distribution of brightness temperature, and a large difference between maximum potential intensity (MPI) and current TC intensity.

The ocean is a major energy source driving TCs (Leipper and Volgenau 1972; Lin et al. 2008), even as TCs cool the sea surface temperature (SST) of the underlying ocean by producing turbulent mixing or upwelling (Leipper 1967; O'Brien and Reid 1967; O'Brien 1967; Price 1981). It has been proposed that a warm upper-ocean structure, namely, large ocean heat content, likely contributes to RI by reducing the magnitude of TC-induced cooling at the ocean surface (e.g., Hong et al. 2000; Shay et al. 2000; Cione and Uhlhorn 2003; Lin et al. 2005, 2008; Wu et al. 2007; Wada 2015). Miyamoto et al. (2017) developed an analytical model of one-dimensional ocean mixing through wind forcing by a TC and a dimensionless quantity representing the magnitude of TC-induced cooling.

Kaplan et al. (2015) showed that the relative importance of parameters differs between the Atlantic and the eastern North Pacific. Although statistical studies have been conducted on data from the Atlantic and the eastern North Pacific, few statistical studies have examined RI-TCs in the western North Pacific (WNP), which is the most active TC region in the world. To our knowledge, two statistical studies of the WNP focusing on RI-TCs were by Wang et al. (2015) and Hendricks et al. (2010, hereafter H10). Wang et al. (2015) investigated the multidecadal variability of RI events in the WNP, but they did not study annual changes in RI-TC activity and characteristics of RI-TCs. Using a global analysis, H10 found that RI is largely controlled under favorable environmental conditions and that atmospheric conditions in the WNP favor TC intensification. However, H10 did not examine some important features relevant to TCs that have been examined in the statistical and modeling studies cited above, for example, TC structure and ocean heat content. The analysis period for RI-TC in H10 was six years from 2003 to 2008; annual changes in RI-TC activity were not investigated in the study. Furthermore, H10 used a different definition of RI from that widely used in statistical analyses of RI, 30 kt (15.4 m s^{-1}) in a 24-h period: their definition was 38 kt (19.5 m s^{-1}) in a 24-h period for the WNP and 35 kt (18.0 m s^{-1}) in a 24-h period for the Atlantic.

Therefore, in this study we statistically investigated the characteristics of RI-TCs and RI-TCs associated with the environmental physical parameters that influence RI, including both atmospheric and oceanic features. The analysis period was 37 years, from 1979 to 2015, in which annual changes in RI-TC activity were examined. For the analysis, RI was defined as an increase in wind speed of 30 kt or more in a 24-h period.

2. Data

This study examined 900 TCs occurring over the WNP during the 37 years from 1979 to 2015 with tropical storm (TS) intensity or greater, that is, with a maximum sustained wind speed at least 35 kt, as derived from the best track (BT) data created by the Regional Specialized Meteorological Center (RSMC) Tokyo–Typhoon Center of the Japan Meteorological Agency (JMA). To accurately detect RI-TCs, TCs that reached TS intensity over the eastern North Pacific and then entered the WNP were excluded, as well as TCs that retained TS intensity beyond the end time listed in the BT data.

We detected RI-TCs and TCs that did not experience RI (NR-TCs), where RI is defined as an increase in wind speed of 30 kt or more in a 24-h period. Similar to the previous studies (e.g., Kaplan and DeMaria 2003), the frequency distributions of the 24-h intensity changes of 900 TCs were analyzed (Fig. 1). Our threshold corresponds to approximately the 96th percentile, which is similar to the results of Kaplan and DeMaria (2003) for the Atlantic; their RI threshold corresponded to the 95th percentile.

Throughout the lifetime of each TC, we determined the times at which the following events occurred: TS formation (TSF), time at which a TC satisfies the RI definition (RI onset), end time of RI, time when a TC achieves maximum intensity (maturity), and time of decay. The end of RI corresponded to the time at which the development rate no longer satisfied the criteria of the RI definition. The decay time referred to the time at which the intensity is below the TS intensity.

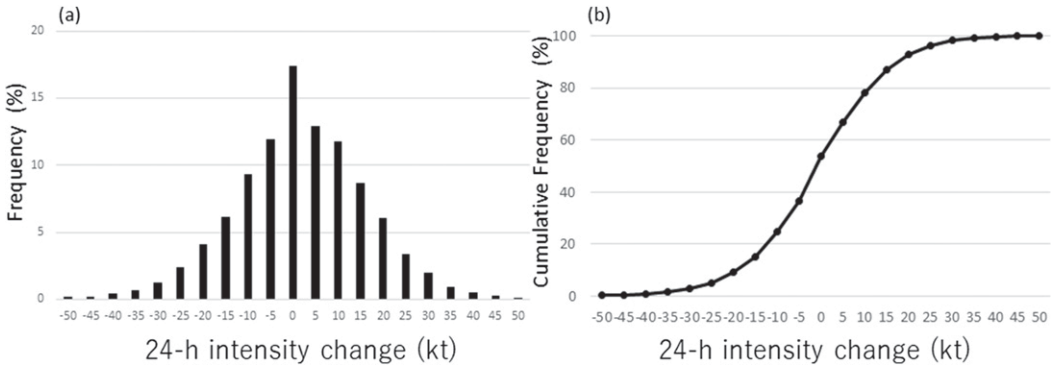

FIG. 1. (a) Occurrence rate and (b) cumulative frequency distributions of 24-h intensity change of TCs over the 37-yr analysis period. This study focused only on TCs that had TS intensity or greater.

In this work, a one-tailed bootstrap-based test with 10 000 resamples and a conventional *t* test were employed to check if the difference in general characteristics of TC structures and environmental parameters between RI-TC and NR-TC is statistically significant. We call the differences "significant" if the confidence level is over 95% in both statistical tests. Statistical TC characteristics, such as location, intensity (a maximum sustained wind speed and central pressure), and size in the horizontal direction (averaged radius of 30-kt sustained wind) were derived from the BT data.

We also investigated differences in environmental physical parameters between RI-TCs and NR-TCs. Atmospheric information was retrieved from the Japanese 55-year Reanalysis (JRA-55; Kobayashi et al. 2015) (details available online at http://jra.kishou.go.jp/JRA-55/index_en.html). JRA-55 collected data every 6 h with a horizontal resolution of 1.25° for both longitude and latitude from 1958 to the present. Oceanic data were derived from the three-dimensional variational-based parent domain output from the Four-Dimensional Variational Ocean Reanalysis for the Western North Pacific (FORA-WNP30; Usui et al. 2017) (details available online at http://synthesis.jamstec.go.jp/FORA). These data have a horizontal resolution of 0.5° for both longitude and latitude, with 54 vertical levels from 0.5- to 6000-m depth and a 6-h time interval from 1982 to 2015. Note that this study did not use the nested high-resolution domain output of the FORA-WNP30 with a horizontal resolution of 0.1° because the nested domain was limited to the area that did not cover the WNP completely.

Using JRA-55 and FORA-WNP30, we evaluated differences in the following environmental physical parameters: magnitude of vertical wind shear, atmospheric relative humidity, MPI, convective available potential energy (CAPE) derived from the MPI equation, SST, tropical cyclone heat potential (TCHP), depth of the 26°C oceanic isotherm, 0–100-m-depth average ocean temperature, and ocean cooling parameter. Atmospheric relative humidity was calculated in atmospheric layers—850–700 (RHLO), 700–500 (RHMD), and 500–300 hPa (RHHI)—within an annulus of 200–800 km from the TC center. As was used in several previous studies (e.g., Knaff et al. 2005), this annular average was used to estimate environmental parameters in this study. To remove the effect of terrain, the averages for parameters were not included over land. The magnitude of vertical wind shear was defined as the difference in horizontal winds between 200 and 850 hPa (SHRD) and between 500 and 850 hPa (SHRS). The zonal components of the vertical wind shear in these layers were also created (USHRD and USHRS, respectively).

The oceanic parameters—SST, TCHP, depth of the 26°C oceanic isotherm, and 0–100-m-depth average ocean temperature—were calculated within a circular area with an 800-km radius from the TC center to stratify distinct features by RI conditions. Statistical analyses for the atmospheric and oceanic parameters were used to associate TCs with each factor over the 34 years from 1982 to 2015, the same as the available period of FORA-WNP30.

We examined the differences in MPI and CAPE between the RI and NR conditions. MPI was originally proposed by Emanuel (1986); the revised version presented by Bister and Emanuel (1998) was used in our study. MPI was calculated from atmospheric data within an annulus of 200–800 km from the TC center over 34 years, the same as the available period of both JRA-55 and FORA-WNP30. To compare atmospheric stability between RI-TC and NR-TC environments, we used E-CAPE, a version of CAPE calculated from the simple equation presented in MPI theory, which is an approximate form [equations are introduced in detail by Emanuel (1994) and Bister and Emanuel (2002)]. E-CAPE was calculated within an annulus of 200–800 km from the TC center.

TCHP was estimated by summing ocean heat content from the surface to the depth of the 26°C isotherm (Leipper and Volgenau 1972; Wada 2015), as follows:

$$Q = C_p \sum_{z=0}^{Z26} \rho_i (T_i - 26) \Delta z_i, \quad (1)$$

where Q is TCHP (kJ cm^{-2}), C_p is specific heat at constant pressure, T_i is water temperature (°C) at the ith level, Δz_i is layer water thickness at the ith level (m), and ρ_i is the density of water at the ith level. The parameter Z26 is the depth (m) of the 26°C isotherm (m). TCHP was calculated within a circular area with an 800-km radius from the TC center over 34 years from FORA-WNP30.

Miyamoto et al. (2017) developed an ocean cooling parameter that is a dimensionless quantity representing the magnitude of ocean cooling by turbulent mixing in the upper ocean caused by wind forcing. The quantity is defined as the ratio of wind forcing (related to wind speed, TC size, and speeds of TC motion) and ocean stability (determined by temperature profile), as follows:

$$C_o = \frac{2F_{ms0}^2 \tau^2}{\rho^2 \alpha g \Gamma h_0^4}, \quad (2)$$

where C_o is the nondimensional ocean cooling parameter, F_{ms0} is the surface momentum flux (kg m^{-1} s^{-2}), τ is the mixing time scale (s), α is the thermal expansion coefficient (K^{-1}), g is gravitational acceleration (m s^{-2}), Γ is the temperature lapse rate below the mixed layer (K m^{-1}), and h_0 is the mixed layer depth (m). The momentum flux is calculated by using MPI and a fixed drag coefficient. The time scale of mixing is defined as the ratio of a size parameter (namely, the RMW and the 30-kt sustained wind) to the speed of TC motion. The definition of the size parameter can be found in Miyamoto et al. (2017), and this study used the average RMW (40 km at the TSF and 25 km at the maturity). The speed of TC motion was defined as the distance from the time to 6 h later. Note that the ocean cooling parameter was calculated below the TC center over 34 years from FORA-WNP30.

3. Results

a. Annual and interannual variation in RI-TC

Among the 900 TCs over the analysis period from 1979 to 2015, 201 RI-TCs (22% of the total) and 699 NR-TCs were detected by our definition. Figure 2 shows the total number of RI-TCs for each month during the analysis period. There was large variability in seasonality among the number of RI-TCs; many of these occurred in summer and autumn. Because this seasonal variation was partly due to seasonal variation among all TC occurrences, we examined the rates of RI-TC occurrence by the monthly total of TCs. The differences in the monthly occurrence rates of RI-TC were low, at a monthly rate of 10%–30% (not shown). Hence, RIs potentially occur throughout the year with relatively low variation of RI-TC occurrence rate in the seasonality.

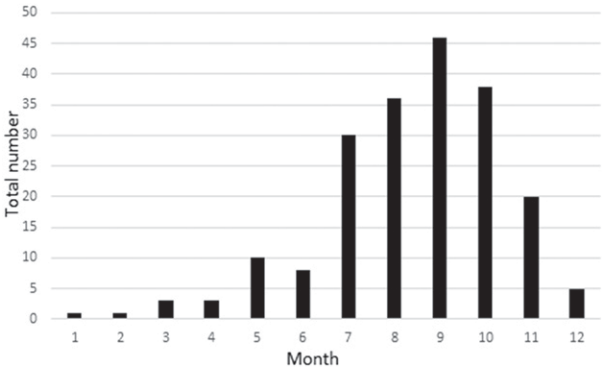

FIG. 2. Monthly total number of RI-TC occurrences over the 37-yr analysis period.

Figure 3 shows the annual number and RI-TC occurrence rate over the WNP from 1979 to 2015. In 2015, 12 RI-TCs was the most frequent number, followed by 10 RI-TCs in 1982 and 2004. In contrast, only one RI-TC was observed in 1988, 1990, and 1999. As shown in Fig. 3b, the RI-TC occurrence rates, the number of RI-TCs divided by the number of TCs per year, varied widely from about 5% to nearly 50%.

Table 1 shows the 5-yr mean of RI-TC occurrence rates from the early 1980s to the early 2010s. The rates of RI-TC occurrence increased from the 1990s to the late 2000s, with a peak in the late 2010s (34%). Ito (2016), counting an RI event from a 6-hourly individual record, reported that the RI occurrence rate had nearly doubled within the past 25 years. The increases of RI-TCs in the late 2000s were also seen in the dataset published by the JTWC (Wang et al. 2015). It could result from a climatological change in the physical parameters that will be investigated in this study or change in the policy of constructing a best track dataset.

The distribution of high SST over the WNP was found to be a key condition determining RI-TC occurrence. It is therefore possible that relatively high/low SSTs over the WNP were related to El Niño–Southern Oscillation (ENSO), resulting in annual variability in the number of RI-TC occurrences. In this study, ENSO years were selected by the JMA definition: El Niño (La Niña) was such that the 5-month running mean SST deviation for Niño-3 (5°S–5°N, 150°–90°W) continues 0.5°C (−0.5°C) or higher (lower) for the summer season from June to

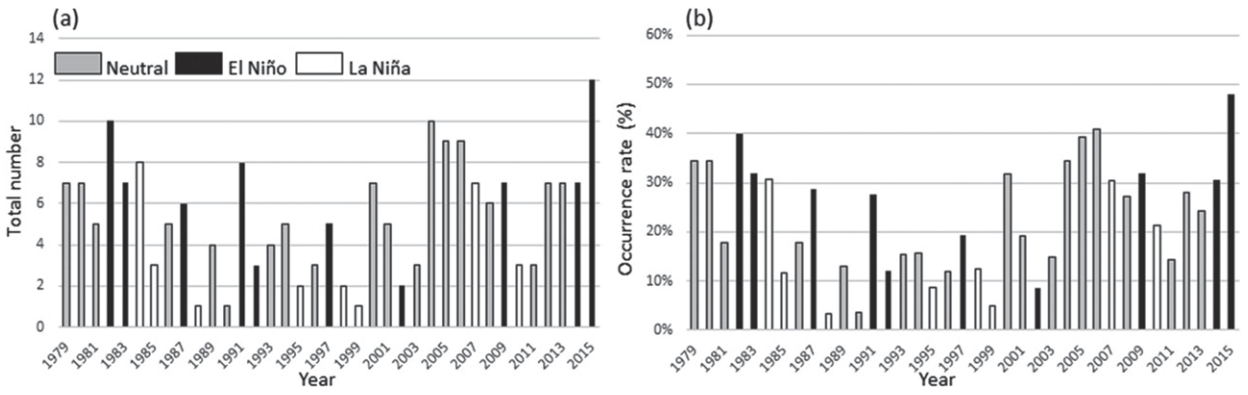

FIG. 3. Annual variation in RI-TC occurrence over the 37-yr analysis period. (a) Number of RI-TCs per year and (b) RI-TC occurrence rates normalized by the annual total. Filled bars indicate El Niño years; white bars are La Niña years; and gray bars are neutral years, when neither phenomenon occurred.

August. There were 10 El Niño years (1982, 1983, 1987, 1991, 1992, 1997, 2002, 2009, 2014, and 2015) and 8 La Niña years (1984, 1985, 1988, 1995, 1998, 1999, 2007, and 2010) (Fig. 3). The average number of annual occurrences (6.7) and the RI-TC occurrence rate (28%) in El Niño years was approximately double those in La Niña years (3.4, 15%). In neutral years when neither phenomenon occurred, the average number of annual occurrences was 5.6 with the RI-TC occurrence rate of 23%.

To avoid the different results provided by the different definitions of ENSO years, this study investigated the annual variability in the RI-TC occurrence number (rate) related to ENSO. As one of the results, the scatter diagram in Fig. 4 shows the relationship between the RI-TC occurrences rate and an annual mean SST deviation for Niño-3. Occurrence rates of RI-TC are higher with increasing annual mean SST deviation. The annual variability in the RI-TC occurrences rate is highly correlated with SST deviation for Niño-3 with a correlation coefficient of 0.41. Thus, TCs in an El Niño year tended to undergo RI, whereas TCs in a La Niña year experienced RI less frequently.

b. *Distribution of RI events*

Figure 5a shows RI onset time from the TSF. A peak in RI onset occurred at 12–18 h after the TSF (19% of the total), followed by 24–30 h (18%) and 36–42 h (16%). The RI onset above 3 days after the TSF was very low. Figure 5b shows the distribution of the RI duration, defined by the period between RI onset and RI end. A 24-h duration was the most frequent (30% of the total), and the number of RI occurrences decreased as RI duration increased. It should be noted that there were no RI-TCs with an RI duration greater than 60 h.

Figure 6 shows the distributions of locations of RI onset. RI was most frequently observed in the elongated region around the eastern Philippine Sea, whereas it was rare for RI to occur in the northern part of the WNP and the South China Sea. This study defined the RI zone at longitudes of 121°–143°E and latitudes of 9°–21°N. The RI zone detected in this study was similar to that reported by H10, which used a different RI definition.

c. *Statistical characteristics of RI-TCs*

This study examined the statistical characteristics of RI-TCs, comparing NR-TC averages at the TSF, the maturity, and the decay. At the TSF, there were no differences in the average intensities of RI-TCs and

TABLE 1. Frequency of occurrence of RI-TCs and NR-TCs, and their respective rates of occurrence. Data are classified into 5-yr intervals.

	RI	NR	RI rate (%)
Early 1980s	37	87	30
Late 1980s	19	116	14
Early 1990s	21	118	15
Late 1990s	13	97	12
Early 2000s	27	93	23
Late 2000s	38	74	34
Early 2010s	27	85	24

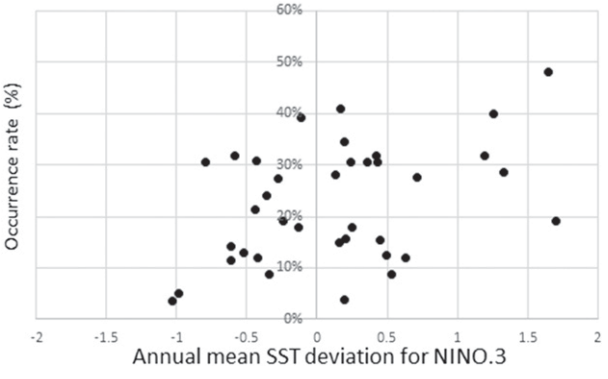

FIG. 4. Scatter diagram showing the relationship between annual mean SST deviation for Niño-3 and RI-TC occurrence rates over the 37-yr analysis period.

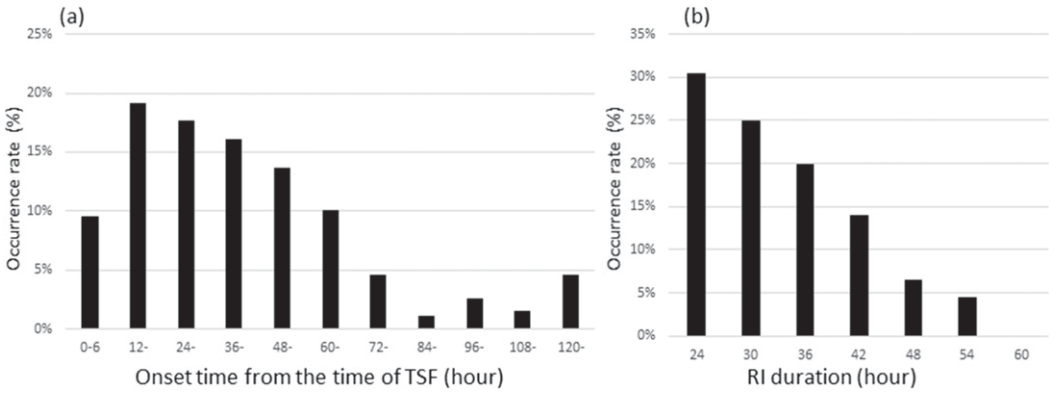

FIG. 5. Occurrence rates of (a) RI onset time from TSF and (b) RI duration between RI onset and RI end over the 37-yr analysis period.

NR-TCs, because all TCs had reached TS intensity by this time. However, the size of TCs in the horizontal direction, defined as the radius of a 30-kt sustained wind, was significantly different (Table 2). The average radius of a 30-kt sustained wind of RI-TCs was smaller than that of NR-TCs. In contrast, the average radius of a 30-kt sustained wind of RI-TCs was significantly larger at the maturity. Because RI-TCs tended to develop into intense TCs to be shown later, an increase in the radius of a 30-kt sustained wind resulted from an increase in the intensity of RI-TCs.

In terms of average intensity, RI-TCs had significantly lower TC central pressure and higher maximum wind. To determine the tendency of an intense TC to develop, we also examined the occurrence of specific classes of TC intensity, defined using the Saffir–Simpson hurricane wind scale (Simpson 1974). During the 37-yr analysis period, 1 category 5 TC [>135 kt (69.5 m s^{-1})], 20 category 4 TCs [114–135 kt (58.6–69.5 m s^{-1})], and 113 category 3 TCs [96–113 kt (49.4–58.1 m s^{-1})] were classed as major TCs, that is, having a maximum wind speed of 96 kt or more. Among 134 major TCs, 101 RI-TCs were detected. To compare the distributions more clearly, the occurrence rates of RI-TCs and NR-TCs were divided by the number of occurrences for major TCs and weak TCs (TS and category 1 TC). The occurrence rate of RI-TCs among major TCs (75%) was 3 times larger than that of NR-TCs (Fig. 7). Conversely, the occurrence rate of RI-TCs among weak TCs was less than 10%. Thus, most RI-TCs developed into major TCs, whereas most NR-TCs remained as weak TCs. These results are consistent with those of a previous study by Kaplan and DeMaria (2003) over the Atlantic, in which most category 4 or 5 hurricanes were found to undergo RI.

d. *Movement and lifetime of RI-TCs*

Figure 8 shows the distributions of occurrence rate of RI-TC and NR-TC locations at the TSF over the 37-yr analysis period. RI-TCs most frequently occurred in the RI zone and southeast of the RI zone, whereas it was rare for RI-TCs to occur in the northern part of the WNP and the South China Sea. Table 2 shows the average locations of RI-TCs and NR-TCs at the TSF. There were significant differences in the average locations at the TSF. RI-TCs occurred on average significantly farther to the east and south than NR-TCs.

Table 2 also shows the direction of TC movements at the TSF, which are determined by the east–west and north–south components of the distances moved between the TSF and 1 day later. NR-TCs tended to be moving northward at the TSF; this trend was significantly different from that of RI-TCs. On the other hand, the east–west component of the movement between RI-TCs and NR-TCs at the TSF did not differ significantly.

Table 2 shows the averages of two measures of TC duration: one is the duration of the development stage from the TSF to the maturity, and the other is the lifespan from the TSF to the decay. The duration of the development stages of RI-TCs and NR-TCs differed significantly. The mean duration of the development

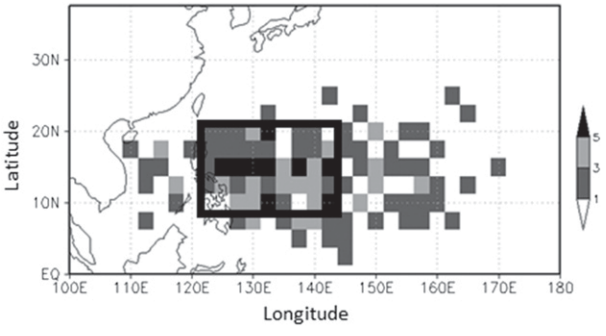

FIG. 6. Locations of the number of RI-TCs at RI onset over the 37-yr analysis period. Box area indicates the RI zone (longitudes of 121°–143°E and latitudes of 9°–21°N).

TABLE 2. Statistical summary of characteristics of RI-TCs (RI) and NR-TCs (NR), and their sum (ALL), over the 37-yr analysis period. Significant differences at the confidence level over 95% in both statistical tests, a one-tailed bootstrap-based test with 10 000 resamples and conventional *t* test, are indicated in italics. Numbers in parentheses are the difference ratios normalizing each variable by subtracting the sample mean and dividing by the standard deviation.

		RI	NR	ALL
Time of TSF	Number	201	699	900
	Avg lat (°N)	*13.9* (−47%)	*16.6* (11%)	16.0
	Avg lon (°E)	*141.7* (46%)	*134.4* (−11%)	136.0
	Radius of 30-kt wind (n mi; 1 n mi = 1.852 km)	*99.2* (−28%)	*115.7* (6%)	112.0
One day after time of TSF	Δlon (°)	−3.1 (−27%)	−2.3 (2%)	−2.5
	Δlat (°)	*1.3* (−30%)	*1.8* (5%)	1.7
Mature time	Duration from TSF (day)	*3.6* (42%)	*2.8* (−10%)	3.0
	Max wind (kt)	*96.1* (189%)	*61.1* (−41%)	68.9
	Min pressure (hPa)	*932.1* (−151%)	*973.3* (42%)	964.1
	Radius of 30-kt wind (n mi)	*252.1* (34%)	*215.1* (−7%)	223.4
Decaying time	Duration from TSF (day)	*5.5* (103%)	*3.8* (−14%)	4.0

stages of RI-TCs was 3.6 days, longer than that of NR-TCs (2.8 days). The longer mean duration of the development stages of RI-TCs was partly due to their tendency to form farther southeastward. The longer duration of the development stage resulted in a longer life-span for RI-TCs than for NR-TCs.

Along the trajectory, we examined the number of landfalls in each country (Japan, China, Vietnam, and the Philippines) (Fig. 9). TC landfall was defined as the intersection of the TC trajectory with a coastline, as described by Fudeyasu et al. (2015). In total, 51 RI-TCs that made landfall in China (including the islands of Taiwan) were the most frequent, followed by the 48 RI-TCs in the Philippines, 34 RI-TCs in Japan, and 19 RI-TCs in Vietnam. The proportion of RI-TCs that made landfall among the total landfall occurrences for each country is shown as a percentage in Fig. 9. The rates of RI-TC occurrence in Japan (33%) and the Philippines (31%) were higher than those in China (22%) and Vietnam (17%).

Table 3 shows characteristics of RI-TCs and NR-TCs that made landfall in each country, the locations of the TSF, the duration from the TSF to landfall, and the intensity at landfall. There were significant differences in the average locations of the TSF between RI-TCs and NR-TCs that made landfall in each country. The average duration of RI-TCs to make landfall in each country was approximately double that of NR-TCs. The average intensity of RI-TCs at landfall in each country was significantly greater than that of NR-TCs. These landfall results will be important in disaster prevention planning for each country.

e. Environmental parameters around RI-TCs

As shown in the previous section, the distributions of RI-TC and NR-TC locations at the TSF are different. To compare the characteristics of environmental parameters among RI-TC and NR-TC correctly, this study considered 67 RI-TCs and 157 NR-TCs that were located in the RI zone at the TSF from July to October over the 34 years from 1982 to 2015, the same as the available period of both JRA-55 and FORA-WNP30. Table 4 shows the averaged atmospheric environmental parameters at the times of the TSF and the maturity, and Table 5 shows the oceanic environmental parameters.

Relative humidity between lower, mid-, and upper troposphere (RHLO, RHMD, and RHHI, respectively) at both the TSF and maturity did not differ significantly, which does not agree with H10. This discrepancy may be related to the detected TCs located in the RI zone at the

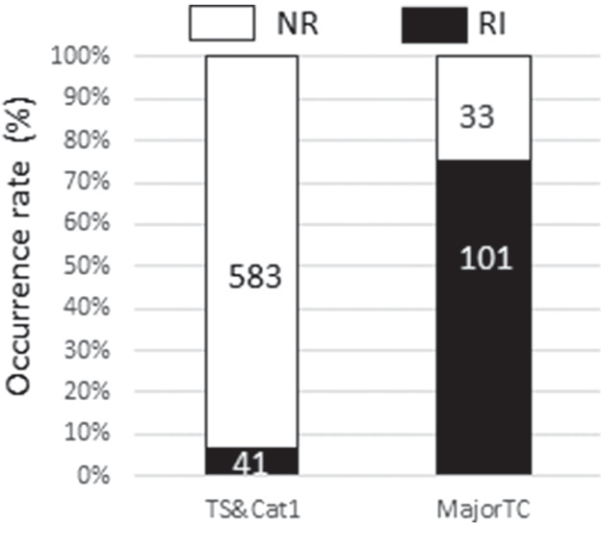

FIG. 7. Occurrence rates of RI-TCs and NR-TCs divided by the number of major TCs (category 3–5 TCs) and weak TCs (TS and category 1 TC) over the 37-yr analysis period. Filled bars indicate RI-TCs.

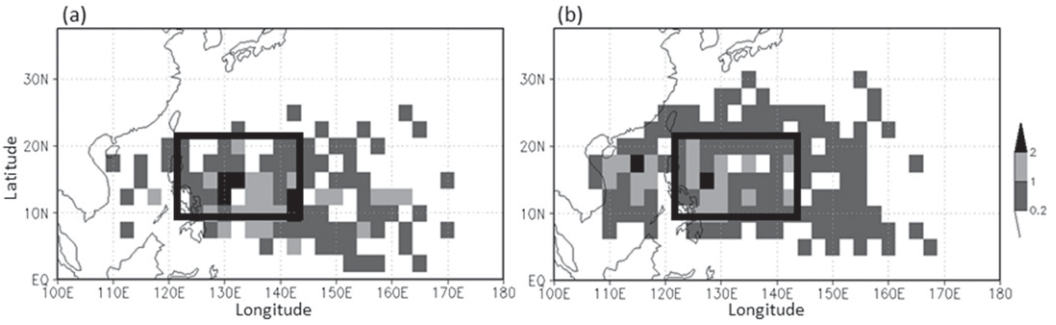

FIG. 8. Locations of occurrence rate of (a) RI-TCs and (b) NR-TCs at the TSF over the 37-yr analysis period. The region of occurrence rate more than 2% is heavily shaded, the region of 1%–2% are lightly shaded, while the region of 0.2%–1% are intermediately shaded. Box area indicates the RI zone.

TSF in summer and autumn in the present study. The vertical wind shears (SHRS, SHRD, USHRS, and UDHRD) of RI-TCs were significantly weaker in RI-TCs at both the TSF and maturity. The E-CAPE and maximum wind speeds derived from the MPI theory were significantly greater in RI-TCs at both the TSF and maturity. According to MPI theory, large-scale environments associated with RI were more favorable for TC development.

There were significant differences in oceanic environmental parameters at both the TSF and maturity (Table 5); TCHP, 0–100-m-depth average temperature, and the 26°C isotherm depth were higher in RI-TCs. These results were consistent with those of previous studies, indicating that higher upper-ocean heat content yielded stronger TCs (e.g., Hong et al. 2000; Shay et al. 2000; Cione and Uhlhorn 2003; Lin et al. 2005, 2008; Wu et al. 2007; Wada 2015). It is interesting to note that the average SST at TSF did not differ significantly between RI-TCs and NR-TCs. At the maturity, the average SST of RI-TCs was significantly higher than that of NR-TCs.

The average ocean cooling parameter at TSF did not differ significantly between RI-TCs and NR-TCs, because the maximum wind speed at the TSF did not differ between RI-TCs and NR-TCs. At maturity, the ocean cooling parameter of RI-TCs was significantly smaller than that of NR-TCs, namely, the small negative effect of TC-induced cooling at the ocean surface in RI-TCs. The difference in speeds of TC motion between RI-TCs and NR-TCs was not also significant at the maturity (not shown), suggesting that the small cooling parameter in RI-TCs at maturity was a result of upper-ocean structure, whereas the size and wind speed of RI-TCs were larger, which tends to increase the cooling parameter.

Differences in the mean value are also shown in Tables 2, 4, and 5. To see the relative importance of each physical variable, we calculated normalized difference ratios, by subtracting the sample mean ($\overline{p}$) from each variable (e.g., p) and dividing by the standard deviation (ρ), that is, $(p-\overline{p})/\rho$. Overall the difference ratios for the vertical wind shears between RI-TCs and NR-TCs were larger at the TSF than at the maturity. In contrast, the difference ratios for the oceanic environmental parameters—CAPE and MPI—were larger at the maturity than at the TSF.

This study examined how the RI zone was connected by the physical environmental parameters. On the ocean east of the Philippines is a broad region of higher SST and E-CAPE, including the RI zone and outside of the RI zone (not shown). Figure 10 shows the distribution of 0–100-m-depth averaged temperature and the zonal component of vertical wind shear between 200 and 850 hPa averaged from July to October. An area of a high 0–100-m-depth averaged temperature more than 28°C extended eastward up to 160°E from east of the Philippines along the latitude of 10°–20°N. The higher vertical wind shear of more than 15 m s^{-1} extended westward up to 140°E from the eastern North Pacific along the latitude of 10°N. The region where the zonal

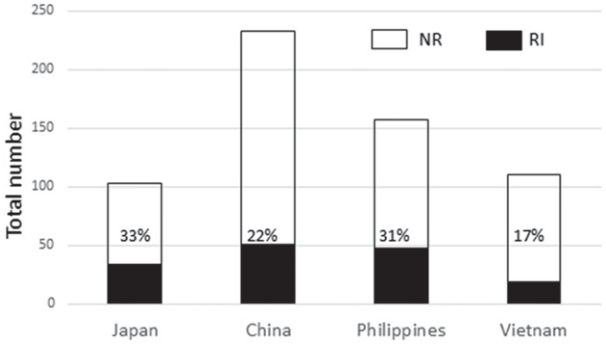

FIG. 9. Number of TCs that made landfall in Japan, China, Vietnam, and the Philippines over the 37-yr analysis period. Filled bars indicate RI-TCs. Percentage values are RI-TC occurrence rates divided by the total number of TCs that made landfall in each country.

TABLE 3. Statistical summary of characteristics of RI-TCs and NR-TCs that made landfall, by country. Significant differences at the confidence level over 95% in both statistical tests, a one-tailed bootstrap-based test with 10 000 resamples and conventional *t* test, are indicated in italics.

		Japan		China		Vietnam		Philippines	
		RI	NR	RI	NR	RI	NR	RI	NR
Time of TSF	All TC	34	69	51	182	19	92	48	109
	Avg lat (°N)	*13.6*	*19.4*	*15.5*	*17.0*	*12.3*	*14.8*	11.2	12.2
	Avg lon (°E)	*146.9*	*136.1*	*135.6*	*125.8*	*135.6*	*119.0*	*138.7*	*133.8*
Landfall	Duration from TSF (day)	*8.2*	*4.5*	*5.7*	*3.6*	*6.5*	*3.3*	*3.7*	*2.6*
	Max wind (kt)	*71.4*	*57.4*	*61.7*	*51.4*	*53.9*	*47.4*	*84.3*	*59.8*
	Min pressure (hPa)	*960.8*	*975.9*	*967.0*	*977.5*	*975.5*	*982.8*	*939.9*	*972.4*

component of weak vertical wind shear overlapped with the higher 0–100-m-depth averaged temperature east of the Philippines is consistent with the RI zone.

4. Discussion

The annual variation in RI-TC activity in the WNP over 37 years was investigated in this study. Although we examined how atmospheric and oceanic environmental physical parameters using JRA-55 and FORA-WNP30 are related to the annual variation in RI-TC occurrence, we did not find high correlation between the annual variation in RI-TC occurrence and environmental parameters (not shown). We consider the uncertainty associated with the atmospheric and oceanic information derived from JRA-55 and FORA-WNP30 caused by nonphysical trends that result from changes in the observing system (e.g., Parker 2016) and the sparsity of observations over the WNP. We need reliable reanalysis data that include both atmosphere and ocean to evaluate environmental physical parameters leading to the long-term trends of RI-TCs. However, we focus on clarifying the characteristics of TC or environmental physical parameters that are favored by the RI events, and the detailed analysis on the long-term scale tendency of each physical parameter or policies is left for future works.

A higher (lower) occurrence rate of RI-TC in El Niño (La Niña) years could be explained by the distribution of TC locations at the TSF. Previous studies (e.g., Wang and Chan 2002) have shown a longitudinal shift in the mean TC locations at the TSF during ENSO years: in El Niño (La Niña) years, more TCs tend to form in the east (west) than in the TC formation location by the climatological mean. Chen et al. (1998) showed that the frequency of TC formation during the summer from June to August in El Niño (La Niña) years increased (decreased) in the southern part of the WNP.

Figure 11 shows the distribution of locations of TCs at the TSF in El Niño and La Niña years. Locations of

TABLE 4. As in Table 2, but for atmospheric environmental physical parameters around RI-TCs and NR-TCs that are located in the RI zone at the TSF in summer and autumn from July to October over the 34 years from 1982 to 2015.

		RI	NR	ALL
TSF time	RHLO (%)	90.8 (−30%)	91.0 (9%)	90.9
	RHMD (%)	81.7 (−15%)	82.0 (6%)	81.9
	RHHI (%)	54.9 (−20%)	56.0 (8%)	55.7
	SHRS ($m\,s^{-1}$)	*2.4* (−32%)	*3.1* (12%)	2.9
	SHRD ($m\,s^{-1}$)	*5.9* (−44%)	*8.0* (16%)	7.0
	USHRS ($m\,s^{-1}$)	*2.4* (−32%)	*3.1* (12%)	2.9
	USHRD ($m\,s^{-1}$)	*5.4* (−36%)	*7.6* (14%)	7.0
	E-CAPE ($J\,kg^{-1}$)	*15 092.8* (35%)	*14 553.5* (−15%)	14 716.4
	MPI max wind ($m\,s^{-1}$)	*124.2* (35%)	*121.8* (−15%)	122.6
Mature time	RHLO (%)	90.8 (−6%)	90.8 (1%)	90.8
	RHMD (%)	81.8 (1%)	82.0 (−5%)	81.9
	RHHI (%)	54.9 (3%)	55.4 (−1%)	55.3
	SHRS ($m\,s^{-1}$)	*3.0* (−23%)	*3.7* (9%)	3.5
	SHRD ($m\,s^{-1}$)	*6.8* (−31%)	*8.6* (11%)	8.1
	USHRS ($m\,s^{-1}$)	*3.0* (−27%)	*3.7* (9%)	3.5
	USHRD ($m\,s^{-1}$)	*5.9* (−23%)	*7.6* (9%)	7.1
	E-CAPE ($J\,kg^{-1}$)	*19 035.3* (93%)	*14 013.4* (−41%)	15 529.9
	MPI max wind ($m\,s^{-1}$)	*138.5* (101%)	*117.8* (−32%)	124.0

TABLE 5. As in Table 2, but for oceanic environmental physical parameters.

		RI	NR	ALL
TSF time	SST (°C)	29.2 (16%)	29.1 (−7%)	29.2
	TCHP (kJ cm^{-2})	*96.5* (26%)	*87.5* (−13%)	90.2
	26°C depth (m)	*93.6* (27%)	*87.7* (−13%)	89.5
	0–100-m average T (°C)	*28.2* (25%)	*27.8* (−12%)	27.9
	Ocean cooling parameter	1.6 (−15%)	2.0 (6%)	1.8
Mature time	SST (°C)	*28.6* (38%)	*28.1* (−10%)	28.3
	TCHP (kJ cm^{-2})	*59.1* (34%)	*45.7* (−21%)	50.5
	26°C depth (m)	*68.0* (38%)	*57.6* (−20%)	61.4
	0–100-m average T (°C)	*26.7* (54%)	*25.7* (−15%)	26.1
	Ocean cooling parameter	*4.1* (−160%)	*7.5* (5%)	7.2

RI-TCs at the TSF in both El Niño and La Niña years were mainly in the RI zone, as shown in Fig. 8. In La Niña years, the locations of TCs at the TSF appeared to the north and west of the RI zone, resulting in the decreases in the occurrence rate of RI-TC. In contrast, locations of TCs at the TSF in El Niño years extended east of the RI zone, resulting in the increase in the occurrence rate of RI-TC.

The relationship between the distribution of TC locations at the TSF and the occurrence rate of RI-TCs could be a possible reason for the trend of TCs that make landfall in each country. Figure 12 shows the distribution of TC locations at the TSF stratified by the landfall occurrences for each country. Locations of TCs at the TSF that made landfall in Japan and the Philippines were mainly in the RI zone or southeast of the RI zone, whereas the locations of TCs at the TSF that made landfall in China and Vietnam were partly in the South China Sea; namely, the trend of occurrence rate of RI-TCs that made landfall in each country could be explained by the distribution of TC locations at the TSF.

Fudeyasu et al. (2006) found that TCs that make landfall on the Korean Peninsula or in Japan in El Niño years tended to have a longer life-span and greater intensities. They considered that an increase in the numbers of intense TCs that make landfall on the Korean Peninsula or in Japan in El Niño years could be attributed to an increase in the number of TCs that formed in the southeastern part of the WNP. Although Fudeyasu et al. (2006) did not focus on TCs that experience RI, trends of intense TCs that made landfall on the Korean Peninsula or in Japan related to ENSO years were similar to the statistical characteristics of RI-TCs provided by this study.

5. Conclusions

We conducted a statistical investigation of the characteristics of TCs undergoing RI in the WNP associated with environmental parameters that are known to influence RI, using records of 900 TCs that occurred over the WNP during the 37 years from 1979 to 2015. Among

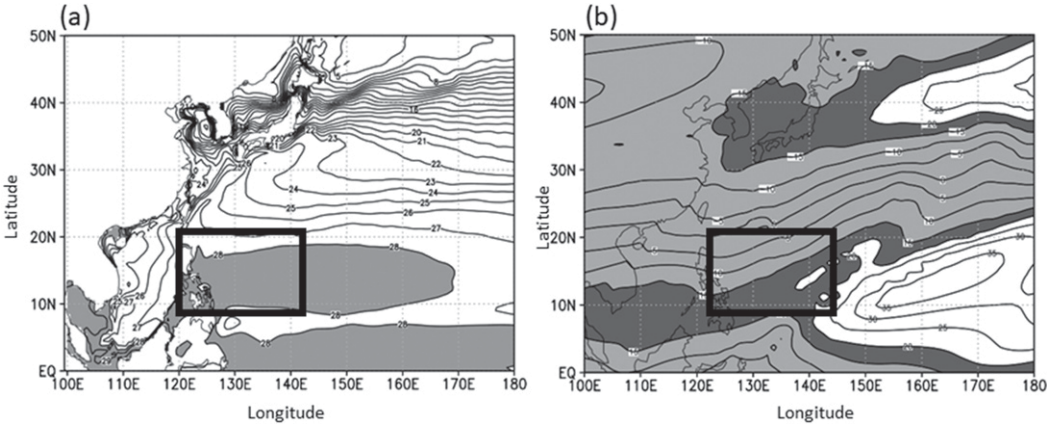

FIG. 10. Distribution of (a) 0–100-m-depth average temperature and (b) zonal components of vertical wind shear between 200 and 850 hPa, averaged from July to October over 34 years from 1982 to 2015. Contour intervals are (a) 1°C and (b) 5 m s^{-1}. Shading in (a) indicates a region larger than 28°C. The region with a vertical shear of 10–15 m s^{-1} in (b) is heavily shaded, while the region less than 10 m s^{-1} is lightly shaded. Box area indicates the RI zone.

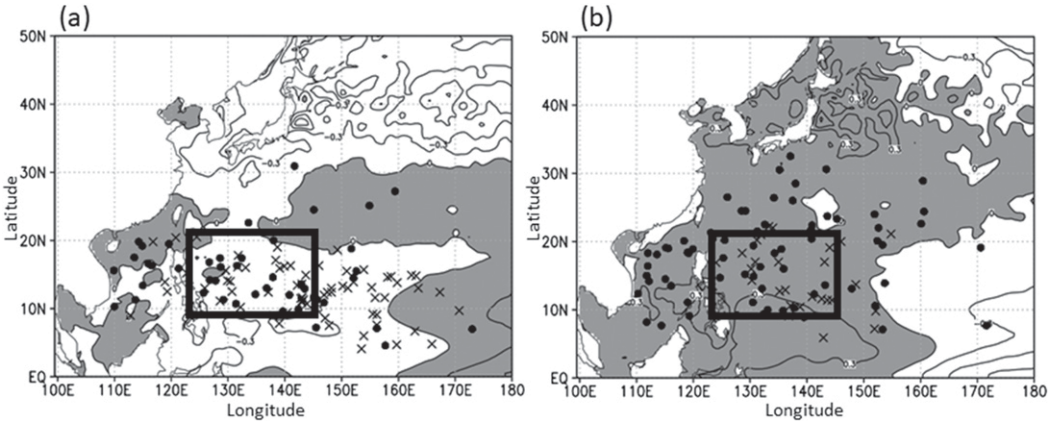

FIG. 11. Distribution of TC locations at the TSF and SST anomaly stratified in (a) El Niño and (b) La Niña years over the 37-yr analysis period. Crosses (closed circles) represent the locations of RI-TCs (NR-TCs) at the TSF. The distribution of SST anomaly is averaged from July to September over the 37-yr analysis period. Contour interval is 0.3°C, and shading indicates areas larger than 0°C. Box area indicates the RI zone.

these 900 TCs, 201 RI-TCs met our criteria of a wind speed increase of 30 kt or more in a 24-h period. Our results, comparing characteristics of RI-TCs and NR-TCs, are summarized below.

- RI-TCs can potentially occur throughout the year with low variation in RI-TC occurrence rate among the seasons.
- The annual occurrence rates of RI-TCs are highly variable, from about 5% to nearly 50%.
- The RI is most frequently observed in the elongated region around the eastern Philippines (RI zone; longitudes of 121°–143°E and latitudes of 9°–21°N), which is consistent with regions of high 0–100-m-depth averaged temperature and weak vertical wind shear averaged from July to October.
- The RI onset tends to occur 0–66 h after the TSF, with a peak at 12–24 h.
- The RI duration is typically 1–2 days, with a peak at 24 h. RI does not continue longer than 2.5 days.

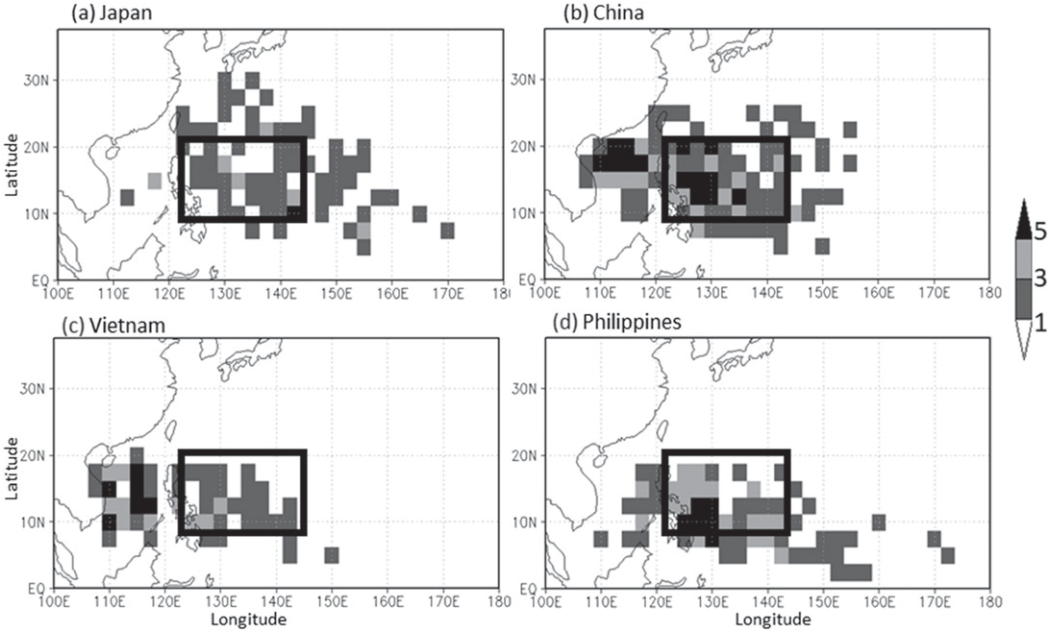

FIG. 12. Distribution of TC locations at the TSF stratified by landfalling in (a) Japan, (b) China, (c) Vietnam, and (d) the Philippines. Box area indicates the RI zone.

- The average location of RI-TCs at the TSF is farther to the east and south than that of NR-TCs.
- TCs in El Niño years tend to undergo RI mainly as a result of the average locations of TCs at the TSF being farther east of the RI zone, whereas TCs in La Niña years experience RI less frequently.
- The rates of RI-TC occurrence increased from the 1990s to the late 2000s, with a peak in the late 2010s.
- The average radius of a 30-kt sustained wind of RI-TCs at the TSF is smaller than that of NR-TCs. In contrast, the average radius of RI-TCs at maturity is larger because of an increase in the intensity of RI-TCs.
- The occurrence rates of RI-TCs that make landfall in Japan and the Philippines are higher than those of RI-TCs in China and Vietnam. The trends in occurrence rate of RI-TCs that made landfall in each country could be explained by the distribution of TC locations at the TSF.
- The development stage and life-span are longer in RI-TCs than in NR-TCs.
- RI-TCs tend to develop as intense TCs as a result of their formation in environments favorable for TC development. Note that with favorable environments for TC intensification, the RI event does not always occur.
- Vertical wind shear is weaker around RI-TCs than NR-TCs at the TSF and maturity.
- Average values of TCHP, 0–100-m-depth average temperature, and depth of the 26°C isotherm of RI-TCs are significantly higher than those of NR-TCs at both the TSF and maturity.
- The average SST and ocean cooling parameters between RI-TCs and NR-TCs at the TSF do not differ significantly, but at the maturity, SST around RI-TCs is higher and the ocean cooling parameter is smaller than that of NR-TCs.
- The difference ratios for the vertical wind shear between RI-TCs and NR-TCs are larger at the TSF than at the maturity. In contrast, the difference ratios for the oceanic environmental parameters, CAPE and MPI, are larger at the maturity than at the TSF.

Studies on the relationship between large-scale environmental parameters that influence RI and annual variability in RI-TC occurrence are needed. Further, the exact reasons why the rates of RI-TC occurrence increased from the 1990s to the late 2000s remain unclear. The statistical characteristics of RI-TCs and large-scale environmental factors, which we investigated in this study, will be useful for climate and TC intensity prediction. In particular, characteristics describing the landfall of RI-TCs in each country will be important for disaster prevention.

Acknowledgments. The authors thank Dr. A. Wada for the helpful comments and support of data analysis. This study utilized the dataset of JRA-55 provided by the Japan Meteorological Agency (JMA). Also this study utilized the dataset of FORA-WNP30, which was kindly provided by the Japan Agency for Marine-Earth Science and Technology (JAMSTEC) and the Meteorological Research Institute of JMA (JMA/MRI). This work is supported by MEXT KAKENHI Grants 17H02956, 16K13884, and Kyoto University Disaster Prevention Research Institute's collaborative research program 29G-05.

REFERENCES

Bister, M., and K. A. Emanuel, 1998: Dissipative heating and hurricane intensity. *Meteor. Atmos. Phys.*, **65**, 233–240, https://doi.org/10.1007/BF01030791.

——, and ——, 2002: Low frequency variability of tropical cyclone potential intensity 1. Interannual to interdecadal variability. *J. Geophys. Res.*, **107**, 4801, https://doi.org/10.1029/2001JD000776.

Chang, C.-C., and C.-C. Wu, 2017: On the processes leading to the rapid intensification of Typhoon Megi (2010). *J. Atmos. Sci.*, **74**, 1169–1200, https://doi.org/10.1175/JAS-D-16-0075.1.

Chen, H., and D.-L. Zhang, 2013: On the rapid intensification of Hurricane Wilma (2005). Part II: Convective bursts and the upper-level warm core. *J. Atmos. Sci.*, **70**, 146–162, https://doi.org/10.1175/JAS-D-12-062.1.

——, and S. G. Gopalakrishnan, 2015: A study on the asymmetric rapid intensification of Hurricane Earl (2010) using the HWRF system. *J. Atmos. Sci.*, **72**, 531–550, https://doi.org/10.1175/JAS-D-14-0097.1.

——, D.-L. Zhang, J. Carton, and R. Atlas, 2011: On the rapid intensification of Hurricane Wilma (2005). Part I: Model prediction and structural changes. *Wea. Forecasting*, **26**, 885–901, https://doi.org/10.1175/WAF-D-11-00001.1.

Chen, T. C., S. P. Weng, N. Yamazaki, and S. Kiehne, 1998: Interannual variations in the tropical cyclone formation over the western North Pacific. *Mon. Wea. Rev.*, **126**, 1080–1090, https://doi.org/10.1175/1520-0493(1998)126<1080:IVITTC>2.0.CO;2.

Cione, J. J., and E. W. Uhlhorn, 2003: Sea surface temperature variability in hurricanes: Implications with respect to intensity change. *Mon. Wea. Rev.*, **131**, 1783–1796, https://doi.org/10.1175//2562.1.

Emanuel, K., 1986: An air–sea interaction theory for tropical cyclones. Part I: Steady-state maintenance. *J. Atmos. Sci.*, **43**, 585–605, https://doi.org/10.1175/1520-0469(1986)043<0585:AASITF>2.0.CO;2.

——, 1994: *Atmospheric Convection.* Oxford University Press, 580 pp.

Fudeyasu, H., and Y. Wang, 2011: Balanced contribution to the intensification of a tropical cyclone simulated in TCM4: Outer core spinup process. *J. Atmos. Sci.*, **68**, 430–449, https://doi.org/10.1175/2010JAS3523.1.

——, S. Iizuka, and T. Matsuura, 2006: Seasonality of westward-propagating disturbances over Southeast and South Asia originated from typhoons. *Geophys. Res. Lett.*, **33**, L10809, https://doi.org/10.1029/2005GL025380.

——, S. Hirose, H. Yoshioka, R. Kumazawa, and S. Yamasaki, 2015: A global view of the landfall characteristics of tropical cyclones. *Trop. Cyclone Res. Rev.*, **3**, 178–192, https://doi.org/10.6057/2014TCRR03.04.

Guimond, S. R., G. M. Heymsfield, and F. J. Turk, 2010: Multiscale observations of Hurricane Dennis (2005): The effects of hot towers on rapid intensification. *J. Atmos. Sci.*, **67**, 633–654, https://doi.org/10.1175/2009JAS3119.1.

Harnos, D. S., and S. W. Nesbitt, 2011: Convective structure in rapidly intensifying tropical cyclones as depicted by passive microwave measurements. *Geophys. Res. Lett.*, **38**, L07805, https://doi.org/10.1029/2011GL047010.

Hendricks, E. A., M. S. Peng, B. Fu, and T. Li, 2010: Quantifying environmental control on tropical cyclone intensity change. *Mon. Wea. Rev.*, **138**, 3243–3270, https://doi.org/10.1175/2010MWR3185.1.

Hong, X., S. W. Chang, S. Raman, L. K. Shay, and R. Hodur, 2000: The interaction between Hurricane Opal (1995) and a warm core ring in the Gulf of Mexico. *Mon. Wea. Rev.*, **128**, 1347–1365, https://doi.org/10.1175/1520-0493(2000)128<1347:TIBHOA>2.0.CO;2.

Ito, K., 2016: Errors in tropical cyclone intensity forecast by RSMC Tokyo and statistical correction using environmental parameters. *SOLA*, **12**, 247–252, https://doi.org/10.2151/sola.2016-049.

——, Y. Ishikawa, Y. Miyamoto, and T. Awaji, 2011: Short-time-scale processes in a mature hurricane as a response to sea surface fluctuations. *J. Atmos. Sci.*, **68**, 2250–2272, https://doi.org/10.1175/JAS-D-10-05022.1.

Jiang, H., 2012: The relationship between tropical cyclone intensity change and the strength of inner-core convection. *Mon. Wea. Rev.*, **140**, 1164–1176, https://doi.org/10.1175/MWR-D-11-00134.1.

Kaplan, J., and M. DeMaria, 2003: Large-scale characteristics of rapidly intensifying tropical cyclones in the North Atlantic basin. *Wea. Forecasting*, **18**, 1093–1108, https://doi.org/10.1175/1520-0434(2003)018<1093:LCORIT>2.0.CO;2.

——, ——, and J. A. Knaff, 2010: A revised tropical cyclone rapid intensification index for the Atlantic and eastern North Pacific basins. *Wea. Forecasting*, **25**, 220–241, https://doi.org/10.1175/2009WAF2222280.1.

——, and Coauthors, 2015: Evaluating environmental impacts on tropical cyclone rapid intensification predictability utilizing statistical models. *Wea. Forecasting*, **30**, 1374–1396, https://doi.org/10.1175/WAF-D-15-0032.1.

Kieper, M., and H. Jiang, 2012: Predicting tropical cyclone rapid intensification using the 37 GHz ring pattern identified from passive microwave measurements. *Geophys. Res. Lett.*, **39**, L13804, https://doi.org/10.1029/2012GL052115.

Knaff, J., C. Sampson, and M. DeMaria, 2005: An operational statistical typhoon intensity prediction scheme for the western North Pacific. *Wea. Forecasting*, **20**, 688–688, https://doi.org/10.1175/WAF863.1.

Kobayashi, S., and Coauthors, 2015: The JRA-55 Reanalysis: General specifications and basic characteristics. *J. Meteor. Soc. Japan*, **93**, 5–48, https://doi.org/10.2151/jmsj.2015-001.

Lee, C.-Y., M. K. Tippett, A. H. Sobel, and S. J. Camargo, 2016: Rapid intensification and the bimodal distribution of tropical cyclone intensity. *Nat. Commun.*, **7**, 10625, https://doi.org/10.1038/ncomms10625.

Leipper, D. F., 1967: Observed ocean conditions and Hurricane Hilda, 1964. *J. Atmos. Sci.*, **24**, 182–196, https://doi.org/10.1175/1520-0469(1967)024<0182:OOCAHH>2.0.CO;2.

Leipper D. F., and D. Volgenau, 1972: Hurricane heat potential of the Gulf of Mexico. *J. Phys. Oceanogr.*, **2**, 218–224, https://doi.org/10.1175/1520-0485(1972)002<0218:HHPOTG>2.0.CO;2.

Lin, I.-I., C.-C. Wu, K. A. Emanuel, I.-H. Lee, C.-R. Wu, and I.-F. Pum, 2005: The interaction of Supertyphoon Maemi with a warm ocean eddy. *Mon. Wea. Rev.*, **133**, 2635–2649, https://doi.org/10.1175/MWR3005.1.

——, ——, I. F. Pun, and D.-S. Ko, 2008: Upper-ocean thermal structure and the western North Pacific category 5 typhoons. Part I: Ocean features and the category 5 typhoons' intensification. *Mon. Wea. Rev.*, **136**, 3288–3306, https://doi.org/10.1175/2008MWR2277.1.

Miller, W., H. Chen, and D.-L. Zhang, 2015: On the rapid intensification of Hurricane Wilma (2005). Part III: Effects of latent heat of fusion. *J. Atmos. Sci.*, **72**, 3829–3849, https://doi.org/10.1175/JAS-D-14-0386.1.

Miyamoto, Y., and T. Takemi, 2013: A transition mechanism for the axisymmetric spontaneous intensification of tropical cyclones. *J. Atmos. Sci.*, **70**, 112–129, https://doi.org/10.1175/JAS-D-11-0285.1.

——, and ——, 2015: A triggering mechanism of rapid intensification of tropical cyclones. *J. Atmos. Sci.*, **72**, 2666–2681, https://doi.org/10.1175/JAS-D-14-0193.1.

——, and D. S. Nolan, 2018: Structural changes preceding rapid intensification in tropical cyclones as shown in a large ensemble of idealized simulations. *J. Atmos. Sci.*, **75**, 555–569, https://doi.org/10.1175/JAS-D-17-0177.1.

——, G. H. Bryan, and R. Rotunno, 2017: An analytical model of maximum potential intensity for tropical cyclones incorporating the effect of ocean mixing. *Geophys. Res. Lett.*, **44**, 5826–5835, https://doi.org/10.1002/2017GL073670.

Molinari, J., and D. Vollaro, 2010: Rapid intensification of a sheared tropical storm. *Mon. Wea. Rev.*, **138**, 3869–3885, https://doi.org/10.1175/2010MWR3378.1.

Nguyen, L. T., and J. Molinari, 2012: Rapid intensification of a sheared, fast-moving hurricane over the Gulf Stream. *Mon. Wea. Rev.*, **140**, 3361–3378, https://doi.org/10.1175/MWR-D-11-00293.1.

Nolan, D. S., and L. D. Grasso, 2003: Nonhydrostatic, three-dimensional perturbations to balanced, hurricane-like vortices. Part II: Symmetric response and nonlinear simulations. *J. Atmos. Sci.*, **60**, 2717–2745, https://doi.org/10.1175/1520-0469(2003)060<2717:NTPTBH>2.0.CO;2.

——, Y. Moon, and D. P. Stern, 2007: Tropical cyclone intensification from asymmetric convection: Energetics and efficiency. *J. Atmos. Sci.*, **64**, 3377–3405, https://doi.org/10.1175/JAS3988.1.

O'Brien, J. J., 1967: The non-linear response of a two-layer, baroclinic ocean to a stationary, axially-symmetric hurricane: Part II. Upwelling and mixing induced by momentum transfer. *J. Atmos. Sci.*, **24**, 208–215, https://doi.org/10.1175/1520-0469(1967)024<0208:TNLROA>2.0.CO;2.

——, and R. O. Reid, 1967: The non-linear response of a two-layer, baroclinic ocean to a stationary, axially-symmetric hurricane: Part I. Upwelling induced by momentum transfer. *J. Atmos. Sci.*, **24**, 197–207, https://doi.org/10.1175/1520-0469(1967)024<0197:TNLROA>2.0.CO;2.

Parker, W. S., 2016: Reanalyses and observations: What's the difference? *Bull. Amer. Meteor. Soc.*, **97**, 1565–1572, https://doi.org/10.1175/BAMS-D-14-00226.1.

Pendergrass, A. G., and H. E. Willoughby, 2009: Diabatically induced secondary flows in tropical cyclones. Part I: Quasi-steady forcing. *Mon. Wea. Rev.*, **137**, 805–821, https://doi.org/10.1175/2008MWR2657.1.

Price, J. F., 1981: Upper ocean response to a hurricane. *J. Phys. Oceanogr.*, **11**, 153–175, https://doi.org/10.1175/1520-0485(1981)011<0153:UORTAH>2.0.CO;2.

Rappaport, E. N., J.-G. Jiing, C. W. Landsea, S. T. Murillo, and J. L. Franklin, 2012: The Joint Hurricane Test Bed: Its first decade of tropical cyclone research-to-operations activities reviewed. *Bull. Amer. Meteor. Soc.*, **93**, 371–380, https://doi.org/10.1175/BAMS-D-11-00037.1.

Rogers, R. F., P. Reasor, and S. Lorsolo, 2013: Airborne Doppler observations of the inner- core structural differences between intensifying and steady-state tropical cyclones. *Mon. Wea. Rev.*, **141**, 2970–2991, https://doi.org/10.1175/MWR-D-12-00357.1.

——, J. A. Zhang, J. Zawislak, H. Jiang, G. R. Alvey III, E. J. Zipser, and S. N. Stevenson, 2016: Observations of the structure and evolution of Hurricane Edouard (2014) during intensity change. Part II: Kinematic structure and the distribution of deep convection. *Mon. Wea. Rev.*, **144**, 3355–3376, https://doi.org/10.1175/MWR-D-16-0017.1.

Rozoff, C. M., and J. P. Kossin, 2011: New probabilistic forecast models for the prediction of tropical cyclone rapid intensification. *Wea. Forecasting*, **26**, 677–689, https://doi.org/10.1175/WAF-D-10-05059.1.

Schubert, W. H., and J. J. Hack, 1982: Inertial stability and tropical cyclone development. *J. Atmos. Sci.*, **39**, 1687–1697, https://doi.org/10.1175/1520-0469(1982)039<1687:ISATCD>2.0.CO;2.

Shapiro, L. J., and H. E. Willoughby, 1982: The response of balanced hurricanes to local sources of heat and momentum. *J. Atmos. Sci.*, **39**, 378–394, https://doi.org/10.1175/1520-0469(1982)039<0378:TROBHT>2.0.CO;2.

Shay, L. K., G. J. Goni, and P. G. Black, 2000: Effects of a warm oceanic feature on Hurricane Opal. *Mon. Wea. Rev.*, **128**, 1366–1383, https://doi.org/10.1175/1520-0493(2000)128<1366:EOAWOF>2.0.CO;2.

Shimada, U., K. Aonashi, and Y. Miyamoto, 2017: Tropical cyclone intensity change and axisymmetricity deduced from GSMaP. *Mon. Wea. Rev.*, **145**, 1003–1017, https://doi.org/10.1175/MWR-D-16-0244.1.

Simpson, R. H., 1974: The hurricane disaster potential scale. *Weatherwise*, **27**, 169–186, https://doi.org/10.1080/00431672.1974.9931702.

Sitkowski, M., and G. M. Barnes, 2009: Low-level thermodynamic, kinematic and reflectivity fields of Hurricane Guillermo (1997) during rapid intensification. *Mon. Wea. Rev.*, **137**, 645–663, https://doi.org/10.1175/2008MWR2531.1.

Usui, T. Y., and Coauthors, 2017: Four-dimensional variational ocean reanalysis: A 30-year high-resolution dataset in the western North Pacific (FORA-WNP30). *J. Oceanogr.*, **73**, 205–233, https://doi.org/10.1007/s10872-016-0398-5.

Vigh, J. L., and W. H. Schubert, 2009: Rapid development of the tropical cyclone warm core. *J. Atmos. Sci.*, **66**, 3335–3350, https://doi.org/10.1175/2009JAS3092.1.

Wada, A., 2015: Verification of tropical cyclone heat potential for tropical cyclone intensity forecasting in the western North Pacific. *J. Oceanogr.*, **71**, 373–387, https://doi.org/10.1007/s10872-015-0298-0.

Wang, B., and J. C. L. Chan, 2002: How strong ENSO events affect tropical storm activity over the western North Pacific. *J. Climate*, **15**, 1643–1658, https://doi.org/10.1175/1520-0442(2002)015<1643:HSEEAT>2.0.CO;2.

Wang, H., and Y. Wang, 2014: A numerical study of Typhoon Megi (2010). Part I: Rapid intensification. *Mon. Wea. Rev.*, **142**, 29–48, https://doi.org/10.1175/MWR-D-13-00070.1.

Wang, X., C. Wang, L. Zhang, and X. Wang, 2015: Multidecadal variability of tropical cyclone rapid intensification in the western North Pacific. *J. Climate*, **28**, 806–3820, https://doi.org/10.1175/JCLI-D-14-00400.1.

Wu, C. C., C. Y. Lee, and I.-I. Lin, 2007: The effect of the ocean eddy on tropical cyclone intensity. *J. Atmos. Sci.*, **64**, 3562–3578, https://doi.org/10.1175/JAS4051.1.

Zawislak, J., H. Jiang, G. R. Alvey III, E. J. Zipser, R. F. Rogers, J. A. Zhang, and S. N. Stevenson, 2016: Observations of the structure and evolution of Hurricane Edouard (2014) during intensity change. Part I: Relationship between the thermodynamic structure and precipitation. *Mon. Wea. Rev.*, **144**, 3333–3354, https://doi.org/10.1175/MWR-D-16-0018.1.

Zhang, D.-L., and H. Chen, 2012: Importance of the upper-level warm core in the rapid intensification of a tropical cyclone. *Geophys. Res. Lett.*, **39**, L14813, https://doi.org/10.1029/2011GL050578.